NEURAL REGENERATION RESEARCH
June 2014, Volume 9, Issue 11
www.nrronline.org

Heavy ion and X-ray irradiation alter the cytoskeleton and cytomechanics of cortical neurons

Yuting Du[1, 2], Jie Zhang[2, 1], Qian Zheng[1], Mingxin Li[1], Yang Liu[3], Baoping Zhang[4], Bin Liu[2, 1], Hong Zhang[3], Guoying Miao[5]

1 School of Stomatology, Lanzhou University, Lanzhou, Gansu Province, China
2 School of Nuclear Science and Technology, Lanzhou University, Lanzhou, Gansu Province, China
3 Department of Radiation Biology and Medicine, Institute of Modern Physics, Chinese Academy of Sciences, Lanzhou, Gansu Province, China
4 School of Civil Engineering and Mechanics, Lanzhou University, Lanzhou, Gansu Province, China
5 Gansu Provincial Hospital, Lanzhou, Gansu Province, China

Yuting Du and Jie Zhang equally contributed to this work.

Corresponding author:
Bin Liu, Ph.D., School of Nuclear Science and Technology, Lanzhou University, Lanzhou 730000, Gansu Province, China; School of Stomatology, Lanzhou University, Lanzhou 730000, Gansu Province, China, liubkq@lzu.edu.cn.
Hong Zhang, Ph.D., Researcher, Department of Radiation Biology and Medicine, Institute of Modern Physics, Chinese Academy of Sciences, Lanzhou 730000, Gansu Province, China, zhangh@impcas.ac.cn.

doi:*10.4103/1673-5374.135315*
http:*//www.nrronline.org/*

Accepted: *2014-05-08*

Abstract

Heavy ion beams with high linear energy transfer exhibit more beneficial physical and biological performance than conventional X-rays, thus improving the potential of this type of radiotherapy in the treatment of cancer. However, these two radiotherapy modalities both cause inevitable brain injury. The objective of this study was to evaluate the effects of heavy ion and X-ray irradiation on the cytoskeleton and cytomechanical properties of rat cortical neurons, as well as to determine the potential mechanism of neuronal injury after irradiation. Cortical neurons from 30 new-born mice were irradiated with heavy ion beams at a single dose of 2 Gy and X-rays at a single dose of 4 Gy; subsequent evaluation of their effects were carried out at 24 hours after irradiation. An immunofluorescence assay showed that after irradiation with both the heavy ion beam and X-rays, the number of primary neurons was significantly decreased, and there was evidence of apoptosis. Radiation-induced neuronal injury was more apparent after X-irradiation. Under atomic force microscopy, the neuronal membrane appeared rough and neuronal rigidity had increased. These cell changes were more apparent following exposure to X-rays. Our findings indicated that damage caused by heavy ion and X-ray irradiation resulted in the structural distortion and rearrangement of the cytoskeleton, and affected the cytomechanical properties of the cortical neurons. Moreover, this radiation injury to normal neurons was much severer after irradiation with X-rays than after heavy ion beam irradiation.

Key Words: *nerve regeneration; radiation brain injury; neurons; heavy ion; X-ray; cytoskeleton; cytomechanical properties; atomic force microscopy; neural regeneration*

Du YT, Zhang J, Zheng Q, Li MX, Liu Y, Zhang BP, Liu B, Zhang H, Miao GY. Heavy ion and X-ray irradiation alter the cytoskeleton and cytomechanics of cortical neurons Neural Regen Res. 2014;9(11):1129-1137.

Introduction

Cranial radiotherapy is one of the most important therapeutic methods for the treatment of various types of primary and metastatic brain tumors (Bhandare and Mendenhall, 2012). Although conventional photon irradiation (including X-rays, ^{60}Co rays and γ-rays) has significantly improved the treatment of cancer, the central nervous system is prone to damage after high-dose irradiation, resulting in severe delayed or progressive nervous tissue injury (Campen et al., 2012; Siegel et al., 2012). Growing evidence from studies has revealed that exposure to irradiation is closely associated with cognitive impairment in brain tumor patients after radiotherapy (Greene-Schloesser et al., 2012; Parihar and Limoli, 2013; Warrington et al., 2013). A heavy ion beam has high linear energy transfer characteristics and it forms a narrow Bragg peak which contributes to a superior biological dose distribution, thus maximizing the range of tumor cells killed. Unlike conventional photons such as X-rays, heavy ion beams have higher relative biological effectiveness and cause severer damage to tumor cells (Kanai et al., 1997; Fokas et al., 2009; Ohno, 2013). Such remarkable biological traits and dose conformity reflect a rationale for the use of heavy ion tumor therapy in the central nervous system.

Despite the fact that high-linear energy transfer heavy ion therapy for brain tumors has improved curative effects relative to conventional X-ray based radiotherapy, severe radiation induced brain injury following this radiotherapy cannot completely be avoided and the toxic effects on normal brain tissue limit its application. The issues regarding brain radiation injury have been widely discussed, and recent investigations have emphasized changes in pathomorphology (Kurita et al., 2001; Valerie et al., 2007; Kim et al., 2008). However, the underlying mechanism remains in debate. Some researchers have presumed that radiation injury is indirectly induced through direct physical damage and the production of free radicals, thus leading to degenerative lesions in the brain tissue (New, 2001; Acharya et al., 2010); while other studies have highlighted the contribution of cell apoptosis caused by DNA injury and changes in the surrounding microenvironment (such as oxidative stress and inflammation) (Okayasu et al., 2009; Kang et al., 2013). However, few studies have focused directly on the investigation of radiation-induced

nerve injury, and radiation damage to the neuronal microstructure and mechanical properties has rarely been evaluated.

The development of microtechniques allows the possibility of performing a quantitative study which addresses high-resolution living cell structural and mechanical properties. As a member of a family of scanning probe microscopes, the atomic force microscope is a highly versatile tool for biomechanical evaluation (Alessandrini and Facci, 2005; Dufrêne et al., 2013). It is not only capable of observing static or dynamic samples at the molecular level, but can also obtain high-resolution images of the samples under physiological conditions, including the visualization of cell surface morphology and ultrastructure. The atomic force microscope is used to study the mechanical properties of cells through applied force and to monitor the Young modulus of cells (García and Perez, 2002; Kuznetsova et al., 2007; Taatjes et al., 2013). Evaluation of the topological structure and mechanical properties of each neuron will provide evidence regarding radiation-induced brain injury at the molecular level (Spedden and Staii, 2013).

The aim of the present study was to observe the cytoskeletons and mechanical properties of living cortical neurons in new-born mice after heavy ion and X-ray irradiation. An immunofluorescence assay and atomic force microscopy were used to reveal the possible mechanism concerning neuronal cell damage caused by radiation therapy. This could provide a theoretical basis for effectively improving the protection of normal brain tissue in future cranial radiotherapy.

Materials and Methods

Animals

Healthy male and female BALB/C mice were provided by the Experimental Animal Center of Lanzhou University, China (license No. SCXK (Gan) 2013-0002) within 24 hours after birth. Protocols were performed in accordance with the *Guidance for the Care and Use of Laboratory Animals*, formulated by the Research Ethics Committee of Good Laboratory Practice of Lanzhou University in China.

Primary neuronal culture

The neonatal mice were killed on a superclean bench and sterilized in 70% alcohol for 5 minutes. Then the brains were hemisected, and bilateral cerebral cortices were dissected and cut into 1 mm^3 pieces. Dissected cortices were dissociated using 0.125% trypsin (Gibco, San Diego, CA, USA) at 37°C for 10–15 minutes, and trituration was carried out by pipetting using a Pasteur pipette. When the solution became flocculated, the digestion was terminated using DMEM/F12 complete medium (Sigma Aldrich, St. Louis, MO, USA) containing 10% fetal bovine serum (Themor, Waltham, MA, USA). The cells were mechanically triturated, filtered and prepared into cell suspension. The obtained suspension was centrifuged at 99.17 × *g* for 5 minutes, and then the supernatant was removed. Suspensions of cells were diluted at a concentration of 1×10^5 cells/mL on glass slides pre-coated with poly-L-lysine (Wuhan Boster Biological Engineering, Wuhan, Hubei Province, China) on 35 mm dishes. Cultures were maintained in DMEM/F12 (Sigma-Aldrich) supplemented 10% fetal bovine serum, 5% D-glucose, 50 IU/mL penicillin and 0.05 mg/mL streptomycin for 4 hours. Then the cell medium was changed to serum-free Neurobasal-A medium (Gibco, San Diego, CA, USA) with 1% glutamine (Sigma Aldrich) and 2% B27 supplement (Invitrogen, Carlsbad, CA, USA). The cells were maintained at 37°C in a humidified incubator with 95% air and 5% CO_2. Half of the medium was renewed every 3 days during the culturing period. Cellular growth was observed using an inverted phase contrast microscope (DE20, Zeiss, Oberkochen, Germany), and cells cultured for 7 days were used for the following experiments.

Identification of neurons

Neuron-specific marker microtubule-associated protein 2 was used for immunofluorescence staining to identify cortical neurons. In brief, after the neurons were cultured for 7 days, culture medium was removed, and the cells were washed three times in PBS and fixed in 2 mL of 4% paraformaldehyde at room temperature for 30 minutes. Subsequently, the fixation solution was discarded and the cells were rinsed again with PBS and cultured in blocking solution containing 0.1% TritonX-100, 10% goat serum and 3% bovine serum albumin at 37°C for 40 minutes. After discarding the blocking solution and another wash in PBS, the cells were cultured in rabbit microtubule-associated protein 2 polyclonal antibody (1:200; Santa Cruz Biotechnology, Santa Cruz, CA, USA) at 4°C overnight, and with rhodamine goat anti-rabbit IgG (1:500; Santa Cruz Biotechnology) in the dark for 1.5 hours. The cell nuclei were labeled with 5 μg/mL 6-diamidino-2-phenylindole dihydrochloride (Sigma Aldrich) for 10 minutes, and washed three times in PBS for 5 minutes each wash. The immunofluorescence staining results regarding the cultured cells were photographed using a laser confocal microscope (LSM700, Zeiss) using anti-quench mounting solution. Ten vision fields at 40 × magnification were randomly selected to calculate the ratio of microtubule-associated protein 2-positive cells to DAPI staining cells, to determine the purity of the cultured neurons.

Irradiation using a heavy ion beam or X-rays

After culturing for 7 days *in vitro*, cells were irradiated with a high-linear energy transfer carbon ion beam at an initial energy of 235 MeV/u and an average linear energy transfer of 31.3 keV/μm generated at the Heavy Ion Research Facility in Lanzhou (HIRFL, Institute of Modern Physics, Chinese Academy of Sciences, Lanzhou, Gansu Province, China). Neurons received a single dose of 2 Gy at a dose rate of approximately 0.6 Gy/min.

Correspondingly, other cell cultures were irradiated with 100 kVp X-rays at a single dose of 4 Gy using a Faxitron 43885D X-ray machine (Tucson, AZ, USA) at a dose rate of 1.038 Gy/min.

Immunofluorescence staining of the neuron cytoskeleton

At 24 hours after the neurons were exposed to irradiation using the heavy ion beam or X-rays, the culture medium

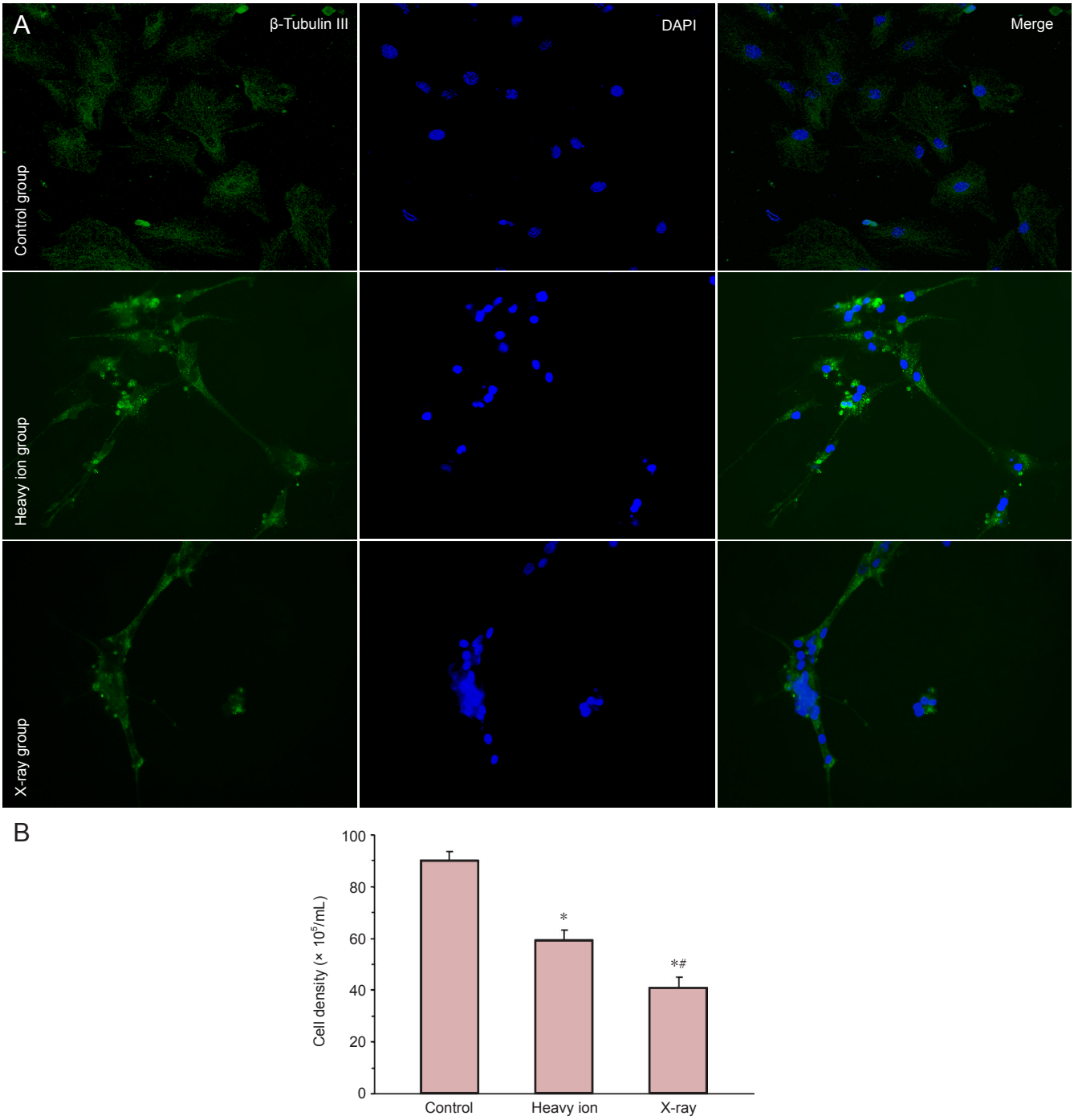

Figure 3 The number of cortical neurons and distribution of cytoskeletal protein after irradiation with heavy ion beam or X-ray irradiation (immunofluorescence staining).
(A) Immunofluorescence assay of neuronal cytoskeleton protein expression at 24 hours after irradiation (× 40). β-Tubulin III stained cytoskeleton (green) and 6-diamidino-2-phenylindole dihydrochloride (DAPI) stained nucleolus (blue); they are merged in the right panel. (B) Quantification of cortical neurons. Data are expressed as mean ± SD. One-way analysis of variance and the two samples *t*-test were applied for comparison between the groups. ∗$P < 0.01$, *vs.* control group; #$P < 0.01$, *vs.* heavy ion group.

was removed and the cells were rinsed three times in PBS for 5 minutes each rinse. Cell cultures were fixed in 4% paraformaldehyde (2 mL; Sigma Aldrich) for 20 minutes at room temperature, followed by a 0.1% TritonX-100 incubation in PBS at 4°C for 10 minutes. Thereafter, cortical neurons were washed in PBS and blocked for 30 minutes in 10% (w/v) goat serum (1:50 in PBS; Sigma) at room temperature. Cultures were again washed with PBS and incubated with primary antibodies (mouse anti-mice β-tubulin III, 1:500, Santa Cruz Biotechnology) at 4°C overnight. The cells were then washed in PBS and incubated with secondary antibody (FITC-conjugated goat anti-rat IgG, 1:500, Santa Cruz Biotechnology) for 1.5 hours in the dark. Then the microtubules were labeled with β-tubulin III and the nuclei were stained

using 6-diamidino-2-phenylindole dihydrochloride. Finally, all fluorescent stained cells were visualized and pictures were captured using a fluorescence microscope (BX53, Olympus, Tokyo, Japan). The neurons that were not irradiated were used as the blank control group.

Atomic force microscope scanning

The three-dimensional topography and mechanical properties of the cells were measured using a NanoWizard III atomic force microscope (JPK, Berlin, Germany). The samples were mounted in the JPK liquid cell chamber and the scanning region was positioned using a monitor. Measurements were taken by means of a 100 μm scanner and UL20B silicon carbide probe, at a Poisson's ratio of 0.5 and a nominal spring constant of 2.8 N/m in contact mode. The images obtained were analyzed using JPKSPM data processing software, which was preassembled in an atomic force microscope. Young's modulus was measured by fitting the Hertz model to the acquired forces (Bernick et al., 2011) according to the following formula:

$$F = \frac{4}{3}\frac{E}{(1-\nu^2)}\sqrt{R}\delta^{\frac{3}{2}}$$

Where, F is the force on the bracket, E is the modulus of elasticity (Young's modulus), R is the radius of curvature of the needle tip, ν is the Poisson's ratio (general 0.5) and δ is the depth.

Statistical analysis

Statistical analysis was performed using SPSS 16.0 software (SPSS, Chicago, IL, USA). Data were expressed as mean ± SD. One-way analysis of variance and the two samples *t*-test were used for comparison of the different groups. A P value < 0.05 was considered as being statistically significant.

Results

Identification of the purity of cortical neurons

Immunofluorescence staining revealed that microtubule-associated protein 2 positive products were located in the neuronal cell bodies and axons; glial cells were not stained. After culturing for 7 days, neurons exhibited intact cell bodies which were oval or polygonal in shape; they had a smooth surface and clear boundary, and synapses developed and connected into a dense network of nerve fibers (**Figure 1**). The purity of cultured cortical neurons was calculated as 85 ± 5%. These findings suggested that the primary cells after 7 days in culture were mainly neurons, which could meet the requirements for cell purity in subsequent experiments.

Effects of heavy ion beams and X-ray irradiation on the morphology of cortical neurons

Under the inverted phase contrast microscope, we found that the non-irradiated neuronal cells (control group) exhibited uneven size, their cell bodies were plump and they had variable shapes including tapered, spindle and irregular. The abundant cytoplasm exhibited strong refraction and an obvious glow, while the nucleuses were large, round and looming. Most control neurons displayed an arborizing neurite growth characterized by numerous branching. They were connected with each other and showed typical formations like radial outgrowth and reticulations formed by axons (**Figure 2A**). At 24 hours after irradiation with heavy ions or X-rays, the number of cells and the connections between the cells were decreased in the heavy ion irradiation group. Furthermore, the soma became smaller and cytoplasmic refraction was lower. Most of the cells were clustered and distributed in an uneven manner. In the X-ray irradiation group, the majority of axon connections were fractured. There were more cell debris and cells were sparsely distributed (**Figure 2B, C**).

Effect of heavy ion beam and X-ray irradiation on the number of cortical neurons and cytoskeletal protein

β-Tubulin III is a member of the tubulin protein family, and is located in the cytoplasm of neuronal cells in the central and peripheral nervous system (Niwa et al., 2013). The immunofluorescence staining demonstrated that the control cells spread to the surrounding areas with plump cytoplasm, and a streaked cytoskeleton around the nucleus was clearly visualized. Relative to the control group (top panel, **Figure 3A**), the cell density was decreased significantly ($P < 0.01$; **Figure 3B**) after heavy ion beam irradiation (middle panel, **Figure 3A**). Most of the irradiated neurons became fusiform with cytoplasmic shrinkage and shorter axons, which lessened the contact between cells. Nevertheless, the X-ray irradiated cell density was decreased more dramatically ($P < 0.01$; **Figure 3B**) and a wealth of axonal fractures appeared. In this group (bottom panel; **Figure 3A**), the cortical neuronal cells exhibited shrinking and a lower distribution of microtubules. Furthermore, chromatin condensation and transparent regions appeared in the nuclei, which were the early signs of apoptosis.

Effect of heavy ion beams and X-ray irradiation on the surface topography of cortical neurons

Under the atomic force microscope, the surface of neurons in the control group did not appear to be smooth. The neurons had various shapes including spindle and tapered. The cell bodies were large (> 100 μm in length) and rich in cytoplasm, which had a clear boundary with the nucleus. The height of the nucleus was significantly higher than the surrounding cytoplasm. There were ridge-like protrusions and folded structures on the soma, which indicated an abundant cytoskeleton. However, the topological structures of the neuronal cells irradiated with the heavy ion beam were changed, with increased membrane roughness and a prominent surface. In the X-ray irradiation group, the cytoskeletal protein structures became fuzzy or even collapsed (**Figure 4**).

Effect of heavy ion beam and X-ray irradiation on the rigidity of cortical neurons

The curve analysis using the JPKSPM data processing software revealed that Young's modulus for neuronal cells was increased after irradiation ($P < 0.01$), which indicated the

increment of cellular hardness. As compared with the heavy ion irradiation group, the Young's modulus was increased significantly in the X-ray irradiation group ($P < 0.01$; **Figure 5**).

Discussion

Radiotherapy can directly trigger damage and apoptosis in hippocampal precursor cells, or prevent the proliferation of precursor cells; thus, it can affect the growth and migration of neonatal neurons, reducing the number of neuronal cells, and aggravating cognition and memory dysfunctions (Acharya et al., 2010). Parihar and Limoli (2013) found that the dendrite branches, length and distribution region were reduced in a dose-dependent manner after mice were exposed to cranial radiation at two doses; the number and density of dendritic spines were also decreased. Mizumatsu et al. (2003) found that ionizing radiation inhibits the growth of nerve cells and promotes apoptosis; nerve cell apoptosis reached a peak at 12 hours after X-ray irradiation in the brains of mice. Moreover, only low doses of radiation exposure caused the decrease in the density of basal dendrites in the hippocampal CA1 subfield and dendritic spine in dentate gyrus granule cells, as well as morphological abnormalities (Chakraborti et al., 2012). However, studies regarding the neuronal cytoskeleton and mechanical properties after irradiation have rarely been reported.

The atomic force microscope can obtain the force-distance curve at any point on the sample surface scanned, thus assisting in the determination of the mechanical properties of the samples. Previous studies have undertaken mechanical measurement of cell bodies and the growth cone area in fixed neurons; the elastic modulus of fixed neurons generally ranges from 10 to several hundred kPa. The modulus values are mediated by the type of neurons and the region measured (Xiong et al., 2009; Jiang et al., 2011). The detection of mechanical properties using the atomic force microscope should be performed in living cells, which limits the measurement time and the range of applied force. Cell adhesion is also a contributing factor, because non-adherent cells may migrate to the surrounding areas under the action of the probe, resulting in ineffective measurement (Spedden et al., 2012). Henderson et al. (1992) used the atomic force microscope for the first time to observe the dynamic behavior of the skeleton of glial cells under physiological conditions. Subsequently, Koch et al. (2012) maintained cell viability and stability during the atomic force microscope measurement process, and obtained physiological data including the elastic modulus. However, neurons with a complex structure, vulnerability to mechanical damage and weak adhesion are mostly treated by chemical fixation prior to experimental study. The chemical fixation interventions may bring about some cell biological problems, especially with regard to irradiated neurons under physiological conditions.

The interoperability of the neural network is a basis for the function of the central nervous system (Parekh and Ascoli, 2013). The formation and establishment of such a network requires precise regulation of synaptic growth and simultaneous repair and reconstruction. Neuronal activity, especially synaptic activity, governs the size and morphology of cells, as well as the density of neurites during brain development (Hur et al., 2012; Malak and Akan, 2012). It is generally considered that the cytoskeleton is a major determinant of neuronal morphology and changes in it result in neuronal morphology and axon changes, and is the ultimate cause of neuronal death (Gordon-Weeks and Fournier, 2014). Indeed, during neuronal morphogenesis the cytoskeletal dynamics plays a crucial role in providing forces for neurite elongation and the subsequent stabilization of the formed axons and dendrites (Franze and Guck, 2010; Franze et al., 2013). The main components of the cytoskeleton are microtubules, actin filaments and intermediate filaments (Spedden et al., 2013). The structural and mechanical characteristics of neuronal cells are effected by cytoskeletal elements, the cell nucleus and cytoplasm, and by the interaction between neurons and the extracellular matrix, which is referred to as the adhesion of cell-substrate (Letourneau et al., 1994). Microtubules are important cytoskeletal superstructures, which are implicated in neuronal morphology and function, including vesicle trafficking, neurite formation and differentiation (Ouyang et al., 2013). Microtubules are a core cylinder consisting of α- and β-tubulin monomers. They are highly dynamic structures that undergo rapid transitions between growth and shrinkage states, known as polymerization and depolymerization (Sakakibara et al., 2013). Within neurons, microtubules provide the inner scaffolding for the outgrowth of neurites and also serve as transport pathways for the organelles between neuronal cell bodies and axon endings. Therefore, abnormal expression of microtubule proteins and the rearrangement of microtubule structures are closely related to cell injury and death (Zhang and Cantiello, 2009; Kapitein and Hoogenraad, 2011). Although it is attractive to speculate that microtubules guide the transport within the apoptotic cell cytoplasm, a pharmacological study pointed out that the function of apoptotic microtubules in chromatin positioning is more stable regarding anchorage than motility (Small and Resch, 2005; Blennow et al., 2012). Moss et al. (2006) have shown that actin filaments and microtubules are involved in inducing the initial process of apoptosis. Alternatively, microtubules and actin might play cooperative roles in apoptotic fragmentation, with the dependence on either varying between cell types. When cells separate during cytokinesis, cooperation between these cytoskeletal systems has been observed. Recent studies have suggested that interphase microtubule depolymerisation might contribute to apoptotic events such as Golgi fragmentation, clustering of mitochondria or the arrest of secretory membrane traffic (Gerner et al., 2000; Pelling et al., 2009; Kapus and Janmey, 2013). Under certain conditions, the microtubules participate in the rearrangement of the cytoskeleton and apoptosis through the release of their hidden apoptosis-related genes, which largely depend on regulating a variety of signals (Ndozangue-Touriguine et al., 2008).

β-Tubulin III, an important component of microtubule associated protein, exhibits an alteration in expression after radiation damage, which can directly reveal changes in the

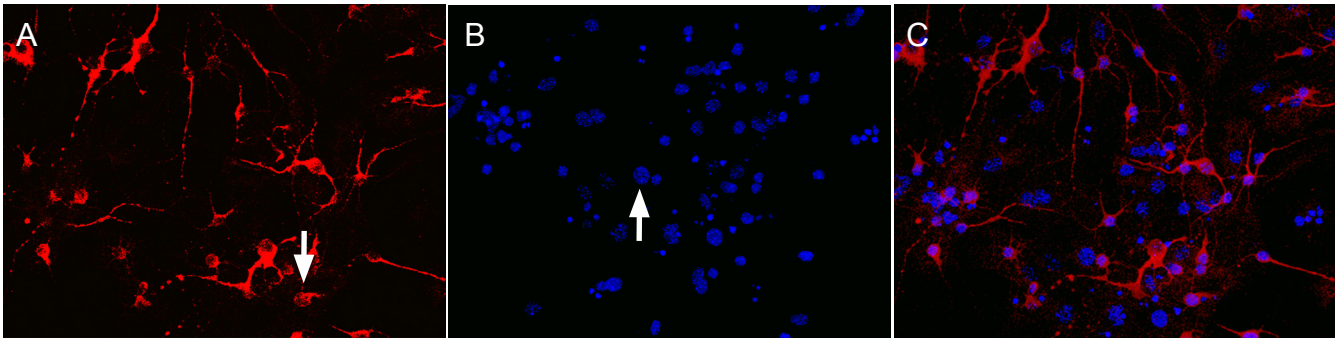

Figure 1 Morphology of cerebral cortical neurons cultured for 7 days (immunofluorescence staining, × 40).
(A) Microtubule-associated protein 2-positive cells (arrow) were stained red; (B) 6-diamidino-2-phenylindole dihydrochloride (DAPI)-stained nuclei (arrow) were stained blue; (C) merged image of A and B.

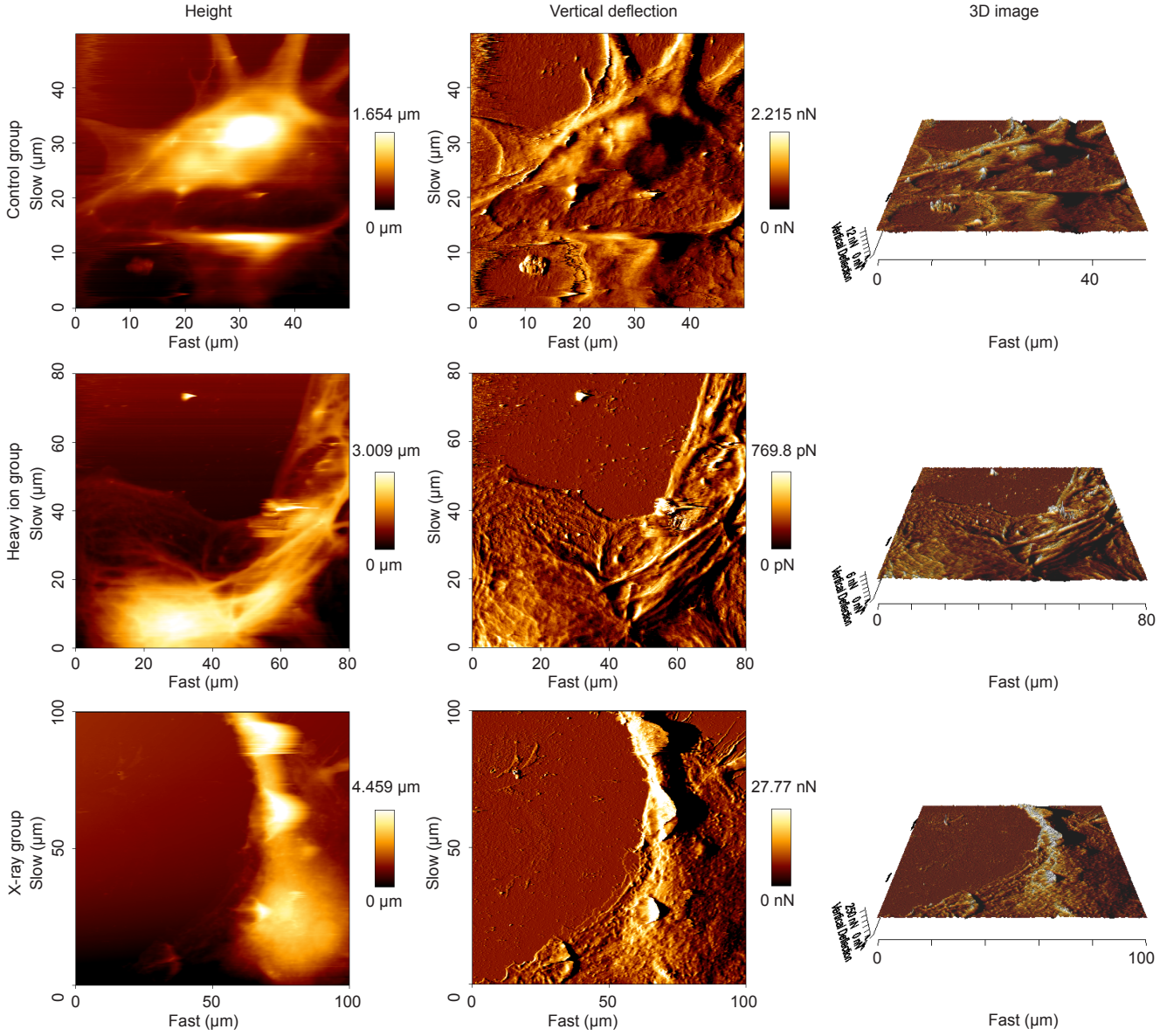

Figure 4 Surface topography of cortical neurons after heavy ion beam or X-ray irradiation (atomic force microscope).
The height graph (left panel): The various colors indicate varying cell heights. Vertical deflection graph (middle panel): The deflection information from the probe during the scanning was recorded to reflect the surface topographical features of the cells, which is more accurate than the height graph. 3D image (right panel): Intuitively reflects the changes in the cell surface. Slow and fast refer to the length and width of the scanning region, respectively.

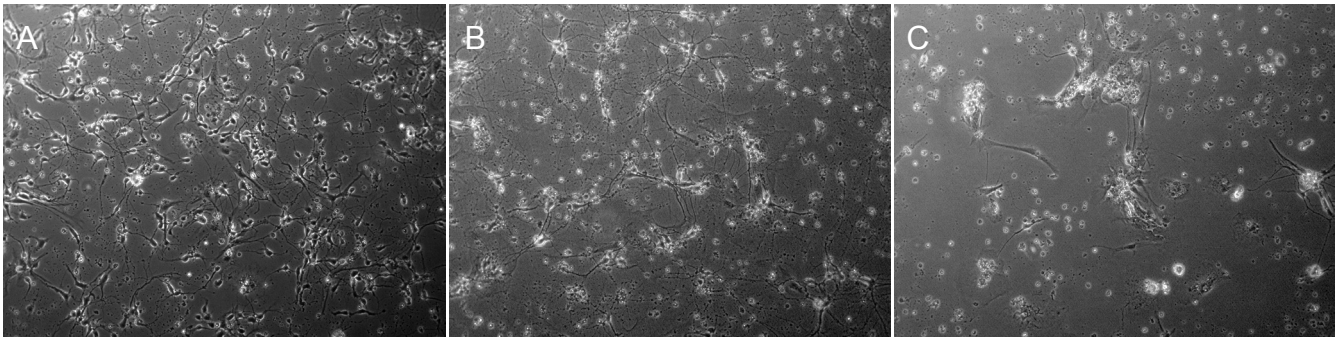

Figure 2 Morphological changes of mouse cortical neurons after heavy ion beam or X-ray irradiation (inverted phase contrast microscope, × 200).
(A) Control group: The morphology of cells is normal. (B) Heavy ion irradiation group: The number of cells is decreased, the soma is smaller and the cytoplasmic refraction is lower. Most of the cells are distributed in an uneven manner. (C) X-ray group: The number of cells is reduced. There is more cell debris and the cells are sparsely distributed.

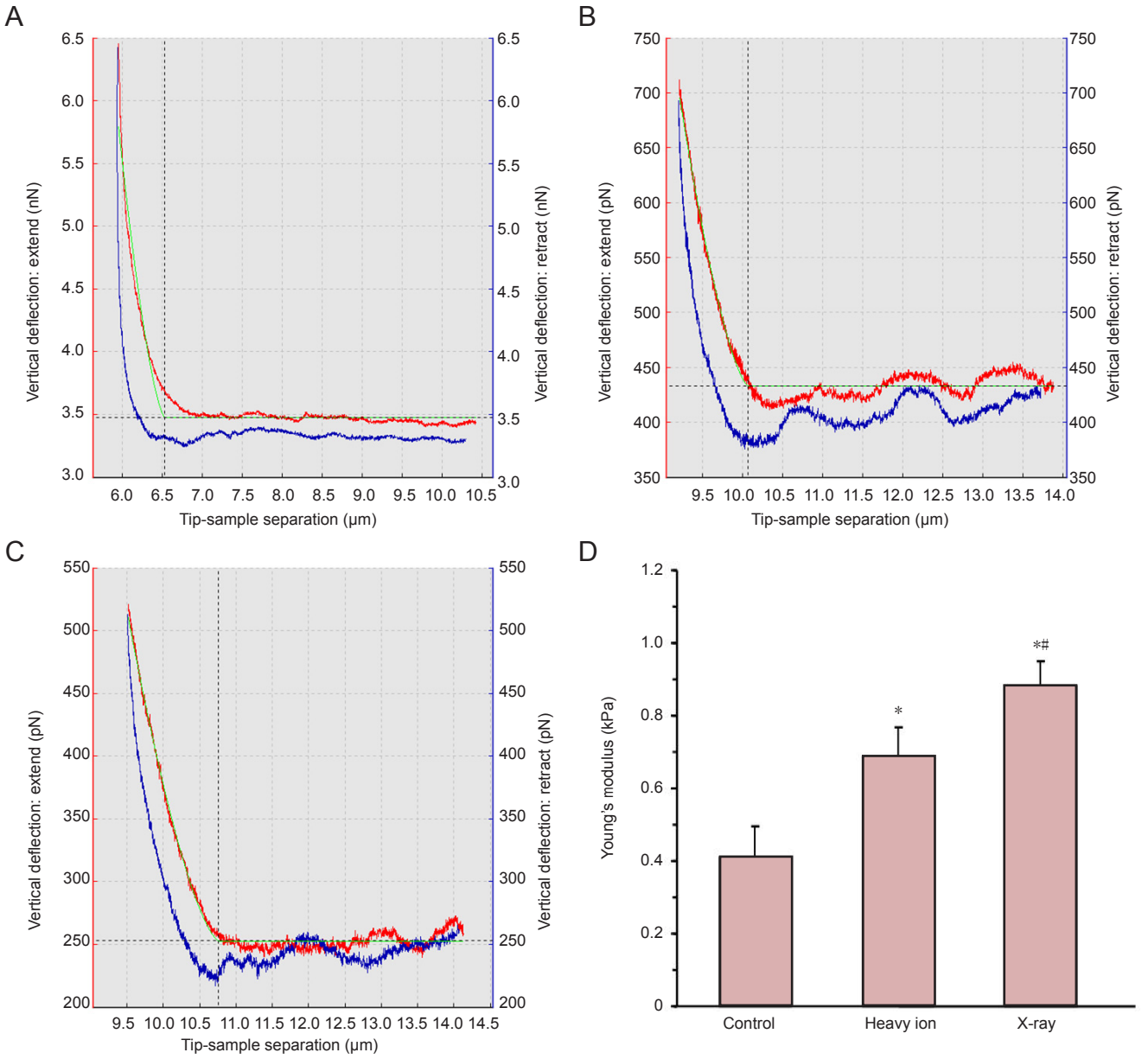

Figure 5 Young's modulus for cortical neurons after heavy ion beam or X-ray irradiation.
(A–C) The force curve for neurons at 24 hours after irradiation detected using an atomic force microscope in contact mode. (A) Control group; (B) heavy ion group; (C) X-ray group. The red curve is the extended curve and the blue curve is the withdrawn curve. The green curve on the red curve was the results of fitting the calculation results of cell elasticity. (D) Data are expressed as mean ± SD. One-way analysis of variance and two samples *t*-test were applied for comparison between the groups. $*P < 0.01$, *vs.* control group; $\#P < 0.01$, *vs.* heavy ion group.

structure of the neuronal cytoskeleton (Brunden et al., 2013). In the present study, immunofluorescence staining indicated that at 24 hours after heavy ion and X-ray irradiation, the cytoskeletal proteins were distributed sparsely and the density of neuronal dendritic spines was also obviously reduced, with the disappearance of reticulate structures. These experimental results provide insight into the types of structural changes induced in the cortical neurons by irradiation, which was related to ion energy in a dose-dependent manner. To our knowledge, the depolymerization, misfolding or denaturation of cytoskeletal proteins might contribute to the destruction of the nutrient transport channel within cells after radiation damage. Moreover, some hidden apoptosis-related genes are released through the regulation of several signals, thus triggering apoptosis and inducing acute radiation injury.

To better understand the mechanical properties of cortical neurons, we used an atomic force microscope to monitor the changes in cell topographies and the dynamics of the cytoskeleton components after irradiation. From the high-resolution images acquired using the atomic force microscope, we found that the normal neurons spread evenly, the cytoskeleton distributed densely near the perinuclear region and scattered gradually and evenly in the cytoplasm, which contributed to maintenance of cell morphology. As compared with the control group, the surface topological structure of the neurons was altered, and the distribution of skeletal structures in the cytoplasm became staggered and even disordered after heavy ion irradiation. In addition, there were more protuberances on the cell surface. In the X-ray irradiated group, the number of cord-like skeletal structures was reduced, cell surface roughness was increased, and some cells even appeared to have pore-like changes forming membrane perforation. All of the above changes implied that irradiation could lead to decomposition and rearrangement of the neuronal cytoskeleton, and that the destruction of the cell membrane protein structure is related to alterations in neuronal skeletal protein structure and function.

Mechanical properties of the cell include elasticity, viscosity and rigidity, which correlate with the cell structure, function and skeletal structure. Alterations in cell elasticity and rigidity are indicators of cell changes in the physiological and pathological processes (Radmacher, 1997). Therefore, the effects of irradiation on the mechanical properties of the neurons can be measured by means of the force-distance curve; the shape of the withdrawn curve reflects the effects of molecule stretching, folding and fracture processes on the cell membrane. The shape of these curves represents the molecular adhesion characteristics of the cell membrane (van der Aa et al., 2001; Pelling et al., 2005). When the cells have received no irradiation, the acting forces between the membrane surface and the probe can be automatically adjusted through surface prestress or tension, so that the surface of the cell membrane becomes relatively smooth, and no adhesion between the cell surface and the probe is formed. After heavy ion and X-ray irradiation, the cell surface becomes rough, skeletal structure is disordered, the ability of self-regulation in response to the probe stimulation is decreased, so the withdrawn curve is irregular and jagged.

Young's modulus, as determined using the atomic force microscope, is a newly acknowledged cellular phenotype characteristic associated with neuronal cells. It is also a mechanical property and can be defined as a quantitative indicator of cell stiffness or elasticity (Pontes et al., 2013). Martin et al. (2013) reported that, as the main cytoskeletal proteins, actin conferred a hard structure while β-tubulin III was responsible for softer material. Another recent study has revealed that, during early apoptosis, the cytoarchitecture is highly dynamic and cells exhibit time-dependent changes in Young's modulus that are clearly dependent on specific apoptotic pathways (Dufrêne and Pelling, 2013). Following radiation injury, our results evidenced an increase in Young's modulus for the cell somas of neurons in radiation induced lesions relative to the control neurons. This increase in Young's modulus revealed a dynamic change in the cytoskeleton and the apparent effect of skeletal rearrangement on cell elasticity. It also indicated an overall hardening of these structures, resulting in severer depolymerization, misfolding or denaturation of microtubules, ultimately leading to a decreased survival rate for cortical neurons.

In conclusion, cranial irradiation can lead to changes in neuronal morphology, and cytoskeletal protein structural disorder may be one of the causes of neuronal morphological change, damage and even apoptosis. Therefore, radiotherapy for brain tumors involving the use of heavy-ion beams or X-rays should be performed carefully at a limited dosage. Our experimental data also revealed that X-rays produced much severer radiation injury to cortical neurons than a heavy ion beam, suggesting that the heavy ion beam has a biological advantage over X-rays in the treatment of malignant tumors and the protection of normal brain tissues. However, the mechanisms involved in the activation of the different signal transduction pathways of cytoskeletal proteins by ionizing radiation, as well as the hidden role of neuronal microtubule-associated proteins in the apoptosis process remain unclear. Hence, additional experimental research is needed in the future.

Author contributions: *All authors were responsible for implementing the experiment and evaluating the experiment. Du YT wrote the manuscript. All authors approved the final version of the manuscript.*
Conflicts of interest: *None declared.*

References

Acharya MM, Lan ML, Kan VH, Patel NH, Giedzinski E, Tseng BP, Limoli CL (2010) Consequences of ionizing radiation-induced damage in human neural stem cells. Free Radic Biol Med 49:1846-1855.

Alessandrini A, Facci P (2005) AFM: a versatile tool in biophysics. Meas Sci Technol 16:R65.

Bernick KB, Prevost TP, Suresh S, Socrate S (2011) Biomechanics of single cortical neurons. Acta biomater 7:1210-1219.

Bhandare N, Mendenhall W (2012) A literature review of late complications of radiation therapy for head and neck cancers: incidence and dose response. J Nucl Med Radiat Ther S2:2.

Blennow K, Hardy J, Zetterberg H (2012) The neuropathology and neurobiology of traumatic brain injury. Neuron 76:886-899.

Brunden KR, Gardner NM, James MJ, Yao Y, Trojanowski JQ, Lee VM-Y, Paterson I, Ballatore C, Smith III AB (2013) MT-stabilizer, dictyostatin, exhibits prolonged brain retention and activity: potential therapeutic implications. ACS Med Chem Lett 4:886-889.

Campen CJ, Kranick SM, Kasner SE, Kessler SK, Zimmerman RA, Lustig R, Phillips PC, Storm PB, Smith SE, Ichord R, Fisher MJ (2012) Cranial irradiation increases risk of stroke in pediatric brain tumor survivors. Stroke 43:3035-3040.
Chakraborti A, Allen A, Allen B, Rosi S, Fike JR (2012) Cranial irradiation alters dendritic spine density and morphology in the hippocampus. PLoS One 7:e40844.
Dufrêne YF, Martínez-Martín D, Medalsy I, Alsteens D, Müller DJ (2013) Multiparametric imaging of biological systems by force-distance curve-based AFM. Nat Methods 10:847-854.
Dufrêne YF, Pelling AE (2013) Force nanoscopy of cell mechanics and cell adhesion. Nanoscale 5:4094-4104.
Fokas E, Kraft G, An H, Engenhart-Cabillic R (2009) Ion beam radiobiology and cancer: time to update ourselves. Biochim Biophys Acta 1796:216-229.
Franze K, Guck J (2010) The biophysics of neuronal growth. Rep Prog Phys 73.
Franze K, Janmey PA, Guck J (2013) Mechanics in neuronal development and repair. Annu Rev Biomed Eng 15:227-251.
García R, Perez R (2002) Dynamic atomic force microscopy methods. Surf Sci Rep 47:197-301.
Gerner C, Fröhwein U, Gotzmann J, Bayer E, Gelbmann D, Bursch W, Schulte-Hermann R (2000) The Fas-induced apoptosis analyzed by high throughput proteome analysis. J Biol Chem 275:39018-39026.
Gordon-Weeks PR, Fournier AE (2014) Neuronal cytoskeleton in synaptic plasticity and regeneration. J Neurochem 129:206-212.
Greene-Schloesser D, Robbins ME, Peiffer AM, Shaw EG, Wheeler KT, Chan MD (2012) Radiation-induced brain injury: A review. Front Oncol 2:73.
Henderson E, Haydon PG, Sakaguchi DS (1992) Actin filament dynamics in living glial cells imaged by atomic force microscopy. Science 257:1944-1946.
Hur EM, Saijilafu, Zhou FQ (2012) Growing the growth cone: remodeling the cytoskeleton to promote axon regeneration. Trends Neurosci 35:164-174.
Jiang FX, Lin DC, Horkay F, Langrana NA (2011) Probing mechanical adaptation of neurite outgrowth on a hydrogel material using atomic force microscopy. Ann Biomed Eng 39:706-713.
Kanai T, Furusawa Y, Fukutsu K, Itsukaichi H, Eguchi-Kasai K, Ohara H (1997) Irradiation of mixed beam and design of spread-out Bragg peak for heavy-ion radiotherapy. Radiat Res 147:78-85.
Kang KA, Lee HC, Lee JJ, Hong MN, Park MJ, Lee YS, Choi HD, Kim N, Ko YG, Lee JS (2013) Effects of combined radiofrequency radiation exposure on levels of reactive oxygen species in neuronal cells. J Radiat Res 55:265-276.
Kapitein LC, Hoogenraad CC (2011) Which way to go? Cytoskeletal organization and polarized transport in neurons. Mol Cell Neurosci 46:9-20.
Kapus A, Janmey P (2013) Plasma membrane--cortical cytoskeleton interactions: a cell biology approach with biophysical considerations. Compr Physiol 3:1231-1281.
Kim JH, Brown SL, Jenrow KA, Ryu S (2008) Mechanisms of radiation-induced brain toxicity and implications for future clinical trials. J Neurooncol 87:279-286.
Koch D, Rosoff WJ, Jiang J, Geller HM, Urbach JS (2012) Strength in the periphery: growth cone biomechanics and substrate rigidity response in peripheral and central nervous system neurons. Biophys J 102:452-460.
Kurita H, Kawahara N, Asai A, Ueki K, Shin M, Kirino T (2001) Radiation-induced apoptosis of oligodendrocytes in the adult rat brain. Neurol Res 23:869-874.
Kuznetsova TG, Starodubtseva MN, Yegorenkov NI, Chizhik SA, Zhdanov RI (2007) Atomic force microscopy probing of cell elasticity. Micron 38:824-833.
Letourneau PC, Condic ML, Snow DM (1994) Interactions of developing neurons with the extracellular matrix. J Neurosci 14:915-928.
Malak D, Akan OB (2012) Molecular communication nanonetworks inside human body. Nano Commun Netw 3:19-35.
Martin M, Benzina O, Szabo V, Végh AG, Lucas O, Cloitre T, Scamps F, Gergely C (2013) Morphology and nanomechanics of sensory neurons growth cones following peripheral nerve injury. PLoS One 8:e56286.
Mizumatsu S, Monje ML, Morhardt DR, Rola R, Palmer TD, Fike JR (2003) Extreme sensitivity of adult neurogenesis to low doses of X-irradiation. Cancer Res 63:4021-4027.
Moss DK, Betin VM, Malesinski SD, Lane JD (2006) A novel role for microtubules in apoptotic chromatin dynamics and cellular fragmentation. J Cell Sci 119:2362-2374.
Ndozangue-Touriguine O, Hamelin J, Bréard J (2008) Cytoskeleton and apoptosis. Biochem Pharmacol 76:11-18.
New P (2001) Radiation injury to the nervous system. Curr Opin Neurol 14:725-734.
Niwa S, Takahashi H, Hirokawa N (2013) β-Tubulin mutations that cause severe neuropathies disrupt axonal transport. EMBO J 32: 1352-1364.
Ohno T (2013) Particle radiotherapy with carbon ion beams. EPMA J 4:9.
Okayasu R, Okada M, Okabe A, Noguchi M, Takakura K, Takahashi S (2009) Repair of DNA damage induced by accelerated heavy ions in mammalian cells proficient and deficient in the non-homologous end-joining pathway. Radiat Res 165:59-67.
Ouyang H, Nauman E, Shi R (2013) Contribution of cytoskeletal elements to the axonal mechanical properties. J Biol Eng 7:21.
Parekh R, Ascoli GA (2013) Neuronal morphology goes digital: a research hub for cellular and system neuroscience. Neuron 77:1017-1038.
Parihar VK, Limoli CL (2013) Cranial irradiation compromises neuronal architecture in the hippocampus. Proc Natl Acad Sci U S A 110: 12822-12827.
Pelling AE, Li Y, Shi W, Gimzewski JK (2005) Nanoscale visualization and characterization of Myxococcus xanthus cells with atomic force microscopy. Proc Natl Acad Sci U S A 102:6484-6489.
Pelling AE, Veraitch FS, Chu CP, Mason C, Horton MA (2009) Mechanical dynamics of single cells during early apoptosis. Cell Motil Cytoskeleton 66:409-422.
Pontes B, Ayala Y, Fonseca ACC, Romão LF, Amaral RF, Salgado LT, Lima FR, Farina M, Viana NB, Moura-Neto V, Nussenzveig HM (2013) Membrane elastic properties and cell function. PLoS One 8:e67708.
Radmacher M (1997) Measuring the elastic properties of biological samples with the AFM. IEEE Eng Med Biol Mag 16:47-57.
Sakakibara A, Ando R, Sapir T, Tanaka T (2013) Microtubule dynamics in neuronal morphogenesis. Open Biol 3:130061.
Siegel R, DeSantis C, Virgo K, Stein K, Mariotto A, Smith T, Cooper D, Gansler T, Lerro C, Fedewa S, Lin C, Leach C, Cannady RS, Cho H, Scoppa S, Hachey M, Kirch R, Jemal A, Ward E (2012) Cancer treatment and survivorship statistics, 2012. CA Cancer J Clin 62:220-241.
Small JV, Resch GP (2005) The comings and goings of actin: coupling protrusion and retraction in cell motility. Curr Opin Cell Biol 17: 517-523.
Spedden E, Kaplan DL, Staii C (2013) High resolution mapping of cytoskeletal dynamics in neurons via combined atomic force microscopy and fluorescence microscopy. In: MRS Proceedings: Cambridge University Press.
Spedden E, Staii C (2013) Neuron biomechanics probed by atomic force microscopy. Int J Mol Sci 14:16124-16140.
Spedden E, White JD, Naumova EN, Kaplan DL, Staii C (2012) Elasticity maps of living neurons measured by combined fluorescence and atomic force microscopy. Biophys J 103:868-877.
Taatjes DJ, Quinn AS, Rand JH, Jena BP (2013) Atomic force microscopy: High resolution dynamic imaging of cellular and molecular structure in health and disease. J Cell Physiol 228:1949-1955.
Valerie K, Yacoub A, Hagan MP, Curiel DT, Fisher PB, Grant S, Dent P (2007) Radiation-induced cell signaling: inside-out and outside-in. Mol Cancer Ther 6:789-801.
van der Aa BC, Michel RM, Asther M, Torrez Zamora M, Rouxhet PG, Dufrêne YF (2001) Stretching cell surface macromolecules by atomic force microscopy. Langmuir 17:3116-3119.
Warrington JP, Ashpole N, Csiszar A, Lee YW, Ungvari Z, Sonntag WE (2013) Whole brain radiation-induced vascular cognitive impairment: mechanisms and implications. J Vasc Res 50:445-457.
Xiong Y, Lee AC, Suter DM, Lee GU (2009) Topography and nanomechanics of live neuronal growth cones analyzed by atomic force microscopy. Biophys J 96:5060-5072.
Zhang P, Cantiello HF (2009) Electrical mapping of microtubular structures by surface potential microscopy. Appl Phys Lett 95:113703.

Copyedited by Morris G, Norman C, Yu J, Yang Y, Li CH, Song LP, Zhao M